in press AGU Geophysical Monograph on the CMB, ed. M. Gurnis, 1998

Three-Dimensional Simulations of Mantle Convection with a Thermo-Chemical Basal Boundary Layer: D"?

Paul J. Tackley

Department of Earth and Space Sciences, University of California, Los Angeles, CA

Numerical simulations in both two- and three-dimensions are performed to investigate the hypothesis that D" is a thermo-chemical boundary layer. A layer of dense, compositionally-distinct material above the CMB reduces the characteristic horizontal lengthscales and interior mantle temperature. In three-dimensions, the layer forms a spoke pattern, with entrainment in upwelling cylinders, even for systems which are heated entirely from within. Long-term stability of the layer requires rather high density contrasts if the Boussinesq approximation is assumed, but geophysically reasonable density contrasts using a compressible formulation with depth-dependent properties. Temperature-dependent viscosity and internal heating also promote greater layer stability. Even if the core heat flux is zero, the layer can become several 100 K higher than the mantle above it, due to trapped radiogenically-produced heat. The combination of high deep-mantle viscosity and other depth-dependent parameters allows a stable layer with very high topography, leading to huge, thermo-chemical 'megaplumes' extending at least half way through the lower mantle. These stationary megaplumes are stable for long geological times and may correspond to the 'megaplumes' imaged tomographically under Africa and the Pacific, as well as acting as a geochemical reservoir and providing an explanation for various other geophysical observations. The dense layer increases the lateral heterogeneity in density and probably seismic velocity in the deep mantle, although the signature of the layer may be partly masked by cancellation of thermal and chemical effects. The interaction of thermal convection with a preexisting dense, homogeneous layer does not cause short-wavelength heterogeneity *per se* (although sharp edges may be generated), and thus some additional mechanism, such as the introduction of fresh heterogeneity by slabs, must be active to explain seismic observations of short-scale D" variation. Unfortunately, these mechanisms tend to produce a layer boundary too gradual to produce a strong seismic reflection, perhaps leading to a phase change as the prefered explanation of the "Lay discontinuity".

INTRODUCTION

The anomalous D" layer at the base of the mantle has been probed by a range of seismic and other geophysical observations (for recent reviews see [*Loper and Lay*, 1995; *Wysession*, 1996]). The layer is characterized by a shear (and possibly P-) wave discontinuity 150 to 450 km above the core-mantle boundary (CMB), a reduced or negative velocity gradient below the discontinuity, and lateral variability on a range of range of lengthscales from ~250 km (e.g., [*Vidale and Benz*, 1993]) to several 1000s km (e.g., [*Su et al.*, 1994; *Masters et al.*, 1996]). While a negative velocity gradient may be expected for a thermal boundary layer, the shear wave discontinuity cannot be generated in this manner, leading to the suggestion of a chemically-distinct dense layer, or a phase transition [*Stixrude and Bukowinski*, 1990; *Nataf and Houard*, 1993]. Recent observations also suggest the presence of a very thin, ultra low-velocity zone immediately above the CMB [*Garnero and Helmberger*, 1996].

In this paper, we investigate the possibility that D" is both chemical and thermal in origin. How could such a dense chemical layer arise? Three possible origins have been proposed: (i) it could be primordial, i.e., formed during the initial differentiation of the Earth, (ii) it could be formed by chemical reactions with the core, producing an iron-rich layer [*Knittle and Jeanloz*, 1989], and (iii) it could be formed by subducted oceanic crust which may segregate from the residuum component when slabs reach the CMB.

The dynamical consequences of a dense chemical layer have previously been investigated using two-dimensional simulations. The formation of plumes from a thermo-chemical boundary layer with temperature-dependent viscosity was modeled by [*Christensen*, 1984], who found that the dense material is readily incorporated in the plume if the ratio of chemical to thermal buoyancy B is less than one, but remained as a stable layer if this ratio is greater than one. This finding was later corroborated by laboratory experiments of two-layered convection [*Olson and Kincaid*, 1991], in which rapid overturn and mixing occurred for

values of B less than one, but stable layering and long-term survival occurred for B greater than one.

If the material remains as a stable layer, a number of things occur. Firstly, the material tends to pile up under upwellings and become thinned under downwellings, with the amount of topography dependent on the Buoyancy ratio. [*Davies and Gurnis*, 1986] found that a dense layer with a density contrast of 2% could result in a discontinuous distribution of material (i.e., zero thickness in places), and cause a bottom topography of several km amplitude, with the CMB depressed under upwellings, the opposite to what is expected from purely thermal convection. These results were corroborated by [*Hansen and Yuen*, 1988] and [*Hansen and Yuen*, 1989] who modeled a more time-dependent system, and also found that the layer could be maintained by a dynamical balance between entrainment and replenishment from the core. Secondly, the dense layer does not survive indefinitely, but is slowly entrained in upwellings, a process which was studied analytically by [*Sleep*, 1988]. Indeed, the analytical models predict that the layer should be completely entrained over geological time, unless its density contrast is at least 6%.

The above models all assume a preexisting layer. Other two-dimensional calculations and one laboratory study have addressed the dynamical feasibility of the two proposed modes of ongoing formation. Can the dense, eclogitic crust of a slab separate out from the thicker, residuum layer when the slab reaches the base of the mantle? This has commonly been modeling by injecting into downwellings two layers of different-density tracers representing oceanic crust and lithosphere, and examining their relative trajectories when they reach the CMB. When the viscosity is constant, the two slab components are unable to separate, and the chemical variations thus give only a small perturbation to the thermal flow [*Gurnis*, 1986]. However, when viscosity is temperature-dependent, segregation of the denser crustal component can indeed occur in the low-viscosity lower boundary layer [*Christensen*, 1989; *Olson and Kincaid*, 1991], and remain there for sufficiently long to explain observed lead and Nd isotope ratios [*Christensen and Hofmann*, 1994]. However, simple mass balance calculations [*Sidorin and Gurnis*, 1998] indicate that the total volume of oceanic crust subducted since the formation of Earth may be too little to account for the observed thickness of the D" layer, particularly since the numerical calculations [*Christensen and Hofmann*, 1994] suggest that only ~20% of the subducted crustal material remains in the layer.

The growth of D" by chemical reactions with the core was modeled by [*Kellogg and King*, 1993], who found that for a buoyancy ratio larger than about 2, a stable layer could form. The required buoyancy ratio is larger than that found in previous studies of a preexisting dense layer probably because the diffusive nature of the formation process causes the composition to change gradually from one extreme to the other, rather than the abrupt change modeled in the studies discussed earlier. A problem with this mode of D" formation is that the reactions are likely to occur only in a very thin layer right at the CMB, with chemical diffusion governing the upwards migration of the material, a very slow process indeed [*Stevenson*, 1993].

In this paper we consider the influence of three-dimensionality on the dynamics of mantle convection with a thermo-chemical D". For these first 3-D results we do not attempt to model the formation of the layer, but simply assume a preexisting layer, and focus on the basic thermal and chemical structures generated, the influence of realistic material properties (e.g., depth-dependent viscosity and other parameters, temperature-dependent viscosity), and the lateral spectrum of heterogeneity at different depths, a quantity which can be directly compared to the heterogeneity spectra from seismic observations.

MODEL

As is common in studies of mantle convection, we make the infinite-Prandtl number approximation and the anelastic-liquid approximation [*Jarvis and McKenzie*, 1980]. The equations, nondimensionalized to the mantle depth (D), thermal diffusion timescale (D^2/κ, where κ=thermal diffusivity) and superadiabatic temperature drop, ΔT_{sa}, are those of continuity:

$$\cdot (\bar{\rho}\underline{v}) = 0 \tag{1}$$

conservation of momentum:

$$\begin{aligned} \cdot \underline{\tau} - \ p &= Ra.(\bar{\alpha}\bar{\rho}T - BC)\ \hat{\underline{z}} \\ \tau_{ij} &= \eta(v_{i,j} + v_{j,i} - \tfrac{2}{3} v_{kk}\delta_{ij}) \end{aligned} \tag{2}$$

conservation of energy:

$$\bar{\rho}\bar{C}_p \frac{DT}{Dt} = -Di_s \bar{\alpha}\bar{\rho}Tv_z + \ \cdot (\bar{k}\ \ T) + \bar{\rho}\bar{H} + \frac{Di_s}{Ra}\tau_{ij}v_{i,j} \tag{3}$$

and conservation of composition:

$$\frac{DC}{Dt} = 0 \tag{4}$$

where the surface dissipation number Di_S is given by:

$$Di_s = \frac{\alpha_s g D}{C_{ps}} \tag{5}$$

v, p, T, C, τ, and η are velocity, dynamic pressure, absolute temperature, composition, deviatoric stress, and dynamic viscosity, respectively, $\underline{z}$ is a unit vector in the vertical direction, and the barred ρ, α, C_p, κ, and k ($=\rho C_p \kappa$) are depth-dependent reference state parameters density, thermal expansivity, heat capacity, thermal diffusivity and thermal conductivity, respectively. These are discussed later. The subscript 's' indicates the surface

value, and the vertical coordinate z runs from 0 at the base to 1 at the surface. The Boussinesq approximation is recovered by setting Di=0 and all depth-dependent properties to 1. The Rayleigh number quoted is based on parameters at the surface, with viscosity (when it is temperature-dependent) defined at the reference adiabat:

$$Ra_s = \frac{\rho_s g \alpha_s \Delta T_{sa} D^3}{\eta(T_{as},0)\kappa_s} \quad (6)$$

where g is the gravitational acceleration, and T_{as} is the surface temperature of the reference adiabat. The Rayleigh number based on properties at the CMB is also quoted.

The chemical composition C varies from 0 to 1. The buoyancy parameter B expresses the ratio of compositional to thermal buoyancy in the system:

$$B = \frac{\Delta\rho_C}{\rho_s \alpha_s \Delta T_{sa}} \quad (7)$$

where $\Delta\rho_c$ is the density difference due to compositional variation, assumed for simplicity to be constant throughout the mantle. The above definition is based on surface parameters; the value based on CMB parameters is also quoted. Note that in equations (1) to (3), chemical variations are neglected except in the buoyancy term of the momentum equation. This is consistent with the Boussinesq or anelastic approximations in which density variations from the reference value are assumed small except in the buoyancy term of the momentum equation, and is justified since B is of order 1. The chemical Rayleigh number Rc used by some authors is simply given by:

$$Rc = Ra.B \quad (8)$$

Viscosity is either constant (η=1), depth-dependent, or temperature- and depth-dependent. For depth-dependent-viscosity cases, the viscosity increases exponentially by a factor of 10 across the mantle depth and discontinuously by a factor of 30 across the 660 km discontinuity (at z=0.7716):

$$\eta(z) = \exp[(1-z)\ln 10].[1 + 29H(0.7716 - z)] \quad (9)$$

where H(x) is the Heavyside step function. The fully temperature- and depth-dependent viscosity law is chosen to give a similar depth-variation along the reference adiabat, plus a strong temperature dependence.

$$\eta(T,z) = A_0 \exp\left\{\frac{27.631 + 11(1-z)}{T + T_{off}}\right\} \quad (10)$$

where A_0 is calculated such that $\eta(T_{as},1) = 1.0$. T_{off} is the temperature offset added to the nondimensional temperature to reduce the otherwise extreme viscosity variation across the upper boundary, and is taken to be 0.88 for compressible cases (this means that the nondimensional surface temperature used in the viscosity law is 1.0, since the surface temperature boundary condition is 0.12). The nondimensional activation energy of 27.631 is the activation energy of dry olivine [*Karato et al.*, 1986], nondimensionalized to the specified temperature scale. To prevent a completely rigid lid from forming [*Solomatov*, 1995; *Ratcliff et al.*, 1997], the maximum viscosity is clipped at 100. Although such clipping may in principle also limit the deep mantle viscosity, in practice the system heats up appreciably when temperature-dependent viscosity is used, so that high viscosity values are not reached in the deep mantle, and this clipping only occurs in the lithosphere. This variation would be reduced if non-Newtonian rheology, which may be important in some regions of the mantle [*Karato and Wu*, 1993], were included, but this is a topic for the future.

Table 1. Thermodynamic parameters: Boussinesq cases

Parameter	Symbol	Value	Units	Non-D value
Input and Derived Parameters				
Depth of mantle	D	2890	km	1.0
Temperature drop	ΔT	2500	K	1.0
Expansivity	α	2.5×10^{-5}	K^{-1}	1.0
Conductivity	k	3.0	$Wm^{-1}K^{-1}$	1.0
Heat capacity	Cp	1200	$J\,kg^{-1}K^{-1}$	1.0
Density	ρ	4000	$kg\,m^{-3}$	1.0
Rayleigh number	Ra	-	-	10^6
Reference visc.	η_{ref}	10^{23}	Pa s	1.0
Nominal Dimensional Conversions				
Velocity	v	1	$cm\,yr^{-1}$	1468
Time	t	424	Gyr	1.0
Heat flux	F	2.6	$mW\,m^{-2}$	1.0
Cond. heat flux	F_{cond}	2.6	$mW\,m^{-2}$	1.0

REFERENCE STATE

A simple thermodynamic model is used to calculate $\rho(z)$ and $\alpha(z)$, with C_p assumed constant, and thermal conductivity $k(z)$ assumed to vary with the fourth power of density [*Anderson*, 1987; *Osako and Ito*, 1991]. The equations are [*Anderson et al.*, 1992; *Duffy and Ahrens*, 1993; *Tackley*, 1996]:

$$\frac{\partial \bar{T}}{\partial z} = -Di.\bar{T} = -Di_s \frac{\bar{\alpha}}{\bar{c}_p}\bar{T}\,; \frac{\partial \bar{\rho}}{\partial z} = -K\bar{\rho} = K_0 \frac{\bar{\alpha}}{\bar{c}_p}\left(\frac{\gamma_0}{\gamma} - \bar{\rho}\right) \quad (11)$$

$$Di = \frac{\alpha g D}{c_p} \quad ; \quad K = \frac{\alpha g D}{\gamma c_p} = \frac{Di}{\gamma} \quad (12)$$

$$\gamma\rho = \text{constant} \quad (13)$$

Table 2. Thermodynamic parameters: compressible cases

Parameter	Symbol	Value	Units	Non-D value
Input and Derived Parameters				
Depth of mantle	D	2890	km	1.0
Surface Dissipation number	Di_S	-	-	1.2
Mean dissipation #	$<Di>$	-	-	0.441
Surface Gruneisen parameter	γ_S	-	-	1.091
Superadiabatic temperature drop	ΔT_{sa}	2500	K	1.0
Surface temperature	T_s	300	K	0.12
CMB Temperature	T_c	3700	K	1.48
Expansivity: surface	α_s	5.0×10^{-5}	K^{-1}	1.0
Conductivity: surface	k_s	3.0	$Wm^{-1}K^{-1}$	1.0
Heat capacity	C_p	1200	$J\ kg^{-1}K^{-1}$	1.0
Density: surface	ρ_s	3300	$kg\ m^{-3}$	1.0
Density: CMB	ρ_b	5467	$kg\ m^{-3}$	1.657
400 density jump	$\Delta\rho_{400}$	280	$kg\ m^{-3}$	0.6784
660 density jump	$\Delta\rho_{660}$	400	$kg\ m^{-3}$	0.9696
Clapeyron slope: 400	γ_{400}	3.0	$MPa\ K^{-1}$	0.0668
Clapeyron slope: 660	γ_{660}	-3.0	$MPa\ K^{-1}$	0.0668
Surface Ra	Ra_s	-	-	10^7
Basal Ra	Ra_b	-	-	3.894×10^3
Reference viscosity	η_{ref}	1.3×10^{22}	Pa s	1.0
Nominal Dimensional Conversions				
Velocity	v	1	$cm\ yr^{-1}$	1211
Time	t	350	Gyr	1.0
Heat flux	F	3.53	$mW\ m^{-2}$	1.0
Conductive heat flux	F_{cond}	8.575	$mW\ m^{-2}$	2.43

$$\alpha = \alpha_0 \exp\left[\frac{\delta_{T0}}{n}\left(1-\left(\frac{\rho_0}{\rho}\right)^n\right)\right] \qquad (14)$$

where γ is the Gruneisen parameter, Di is the dissipation number and K is the compressibility number, $\delta_{T0} = 6.0$, and n=1.4. For the Boussinesq cases, Di=K=0, giving constant coefficients. Thus, in order to construct the non-dimensional reference state, the following surface quantities must be specified: Di_s, T_{as}, K_s and γ_s. This leads to depth variations of ρ, α, and κ, which are all assumed to be 1.0 at the surface. Phase changes at 410 and 660 km depth require specifying a different reference state for each mineral assemblage (from 0-410, 410-660, and 660-2890 km depth). For simplicity, the parameters are taken to be the same, except for the surface density ρ_0 and surface adiabat T_{as} which are chosen to give the PREM density jumps and appropriate adiabatic temperature jumps (due to latent heat) across the two phase transitions.

Table 1 lists assumed parameters for Boussinesq cases (note that since the Boussinesq adiabat is an isotherm, ΔT=ΔT_{sa}), and Table 2 lists parameters for compressible cases, which were chosen to give good fits to PREM density [*Dziewonski and Anderson*, 1981] and thermal expansivity from recent thermodynamic analyses of the lower mantle [*Anderson et al.*, 1992; *Chopelas and Boehler*, 1992; *Duffy and Ahrens*, 1993]. The resulting depth variation of density, temperature, thermal expansivity, thermal conductivity and thermal diffusivity is illustrated in Figure 1.

Dimensional values are also given to allow quantitative comparison of the results with observations. Typical conversions between nondimensional and dimensional heat fluxes and velocities are also given. The Earth's mantle heat flux [*Stacey*, 1992; *Pollack et al.*, 1993] corresponds to 24-28 nondimensional units.

The radiogenic heating rate (assumed constant with time) is chosen so that internally-heated cases have the same surface heat flow as basally-heated cases. For comparison, the heating rate in carbonaceous chondrites, which are usually thought to be representative of mantle material [*Stacey*, 1992] is 5.2×10^{-12} W kg^{-1}, corresponding to 23.2 nondimensional units, which should be reduced to 13.5 nondimensional units in Cartesian geometry to take account of the different surface area:volume ratio [*Tackley*, 1996], but could also be increased to simulate the secular

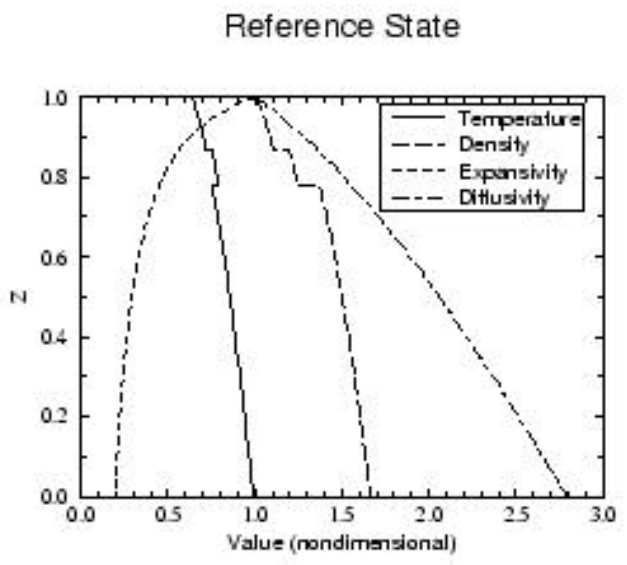

Figure 1. Depth variation of nondimensional reference state parameters temperature, density, thermal expansivity, and thermal diffusivity. The base of the mantle is at z=0, with the top at z=1. Discontinuous jumps are due to the phase transitions at 410 and 660 km depth.

cooling of the mantle, which resembles internal heating both mathematically (in the energy equation) and physically (in its effect on convection) [*Weinstein and Olson*, 1990]. Note that, in the compressible case, the nondimensional heat flux is 2.42 times higher than the Nusselt number, with the latter defined as the ratio of actual heat flux to the conductive heat flux.

NUMERICAL METHOD

The exact details of the numerical method and its benchmarking are described elsewhere [*Tackley*, 1994] and are only briefly summarized here. The instantaneous velocity and pressure fields given by (1)-(3) are calculated by a finite difference (control volume [*Patankar*, 1980]) multigrid technique [*Brandt*, 1982; *Press et al.*, 1992], with vertical grid refinement in the upper and lower boundary layers. Timestepping (equation (4)) is performed explicitly, using the Multidimensional Positive-Definite Advection Transport Algorithm of [*Smolarkiewicz*, 1984] for advection, and second order finite-differences for diffusion, viscous dissipation and adiabatic heating or cooling. Steps of typically 0.5-0.9 the Courant condition are used. The method is well suited to parallel computers, and the presented results were obtained on Intel Paragon and Cray T3E at San Diego Supercomputer Center and the Cray T3E at NASA Goddard Space Flight Center. Benchmarks and accuracy are described in detail in Appendix B of [*Tackley*, 1994].

Phase Transitions. The anomalous buoyancy associated with phase transition deflection is represented as a sheet mass anomaly at the appropriate depth. This technique, previously used by [*Tackley et al.*, 1993; *Tackley et al.*, 1994; *Bunge et al.*, 1997], is similar to the "effective α" approach [*Christensen and Yuen*, 1985] shrunk into a discontinuity. Latent heat release is included in the reference adiabat and is treated numerically by advecting the superadiabatic temperature, rather than absolute temperature. The phase transition implementation has been validated by comparing to previous results, both in a 2-D Cartesian box [*Christensen and Yuen*, 1985], and 3-D spherical shell [*Tackley et al.*, 1994; *Bunge et al.*, 1997].

Chemical field. The denser material is represented by a swarm of tracer particles. For statistical reasons, several 10s of tracers are required per cell [*Christensen and Hofmann*, 1994]. A tracer particle method has the advantages over a continuum field method of having zero chemical diffusion and an ability to represent filaments of material smaller than the grid scale; and the advantages over a marker chain method of being easy to implement (particularly in 3-D) and not growing exponentially in computational cost when the boundary gets complicated [*van Keken et al.*, 1997]. Tracers are advected using a fourth-order Runge-Kutta technique. Chemical buoyancy is computed at each timestep by converting the tracers to the continuum C field using a cell-counting method.

Accuracy becomes an important concern in thermo-chemical convection calculations. [*van Keken et al.*, 1997] present a benchmark for the entrainment of a dense layer at the base of the mantle, and find that for accurate results, the grid resolution must be appreciably higher than that required for thermal convection, and that even then, results computed using different codes diverge after a fairly short time interval. A test of the present code against this benchmark for the period during which all codes obtained the same solution (up to time 0.02) is shown in Figure 2 (directly comparable to Figure 12 in [*van Keken et al.*, 1997]). This figure shows the amount of entrainment vs. time calculated using different resolutions, where the cells are equally-sized in the x-direction but refined in the boundary layers by up to a factor of ~3 in the z-direction. The highest resolution cases (128x64 and 256x64) give similar entrainment vs. time curves to those obtained in the high resolution cases reported in [*van Keken et al.*, 1997], whereas lower resolution leads to unrealistically high entrainment by up to a factor of ~2.5, although the thermal and chemical fields look qualitatively similar. The results did not appear to be particularly sensitive to the number of tracers used.

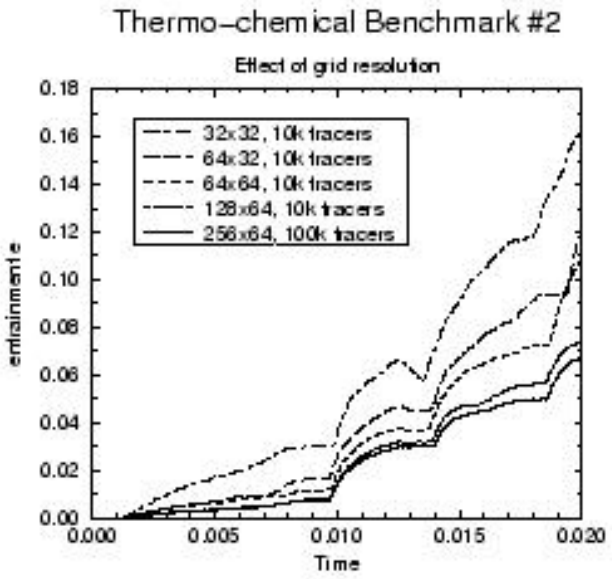

Figure 2. Entrainment vs. time for the thermo-chemical benchmark #2 of [*van Keken et al.*, 1997] (compare with their Figure 12), calculated with various grid resolutions and number of tracer particles. This benchmark models the entrainment of a dense chemical layer. Entrainment 'e' is defined as the fraction of the compositionally dense material that is entrained above z=0.2. The higher resolution results (128x64 or 256x64) are compatible with the high resolution results reported in [*van Keken et al.*, 1997]. Lower resolution results in a higher rates of entrainment, although the convective pattern looks qualitatively similar.

A resolution test has also been performed for a 2-D version of the Boussinesq, basally-heated case presented later in this paper. Plate 1 compares results computed using a 128x32 grid and 25,000 tracers with results computed using a 512x64 grid and 200,000 tracers. As can be seen, the convective patterns look qualitatively the same. However, the rate of entrainment is significantly higher in the lower resolution case, which is why it is shown at an earlier time. One reason for this innacuracy may be the low tracer density (i.e., #tracers per cell) in the filaments of entrained material, the effect of which must be quantitatively determined in the future.

Another aspect of accuracy is the cumulative error in advecting tracer particles, which can be measured by advecting a single particle in a prescribed, steady-state velocity field, for a length of time which should return it to exactly the same position [*van Keken et al.*, 1997]. For the tests described above, and most of the presented results, first-order velocity interpolation was used, giving a cumulative position error of $O(10^{-3})$. When the velocity interpolation was upgraded to second-order, the error dropped to $O(10^{-5})$.

From these tests, it is concluded that: (i) high grid resolution is important if a *quantitatively* accurate entrainment rate is central to the problem being studied, but (ii) the general *qualitative* behavior of the system, e.g., large-scale structure and dynamics, general appearance, is robust with respect to grid resolution. This is also evident in the results presented in figures 8 to 12 in [*van Keken et al.*, 1997].

Since the resources necessary to calculate a suite of 3-D convection calculations with the resolution necessary to accurately capture entrainment rate are not yet available, we must for the moment be satisfied with results which are robust wrt. the general structure and processes, but may overestimate entrainment.

Experimental Procedure

An 8x1 (2-D) or 8x8x1 (3-D) box with periodic side boundaries and free-slip horizontal boundaries was used,

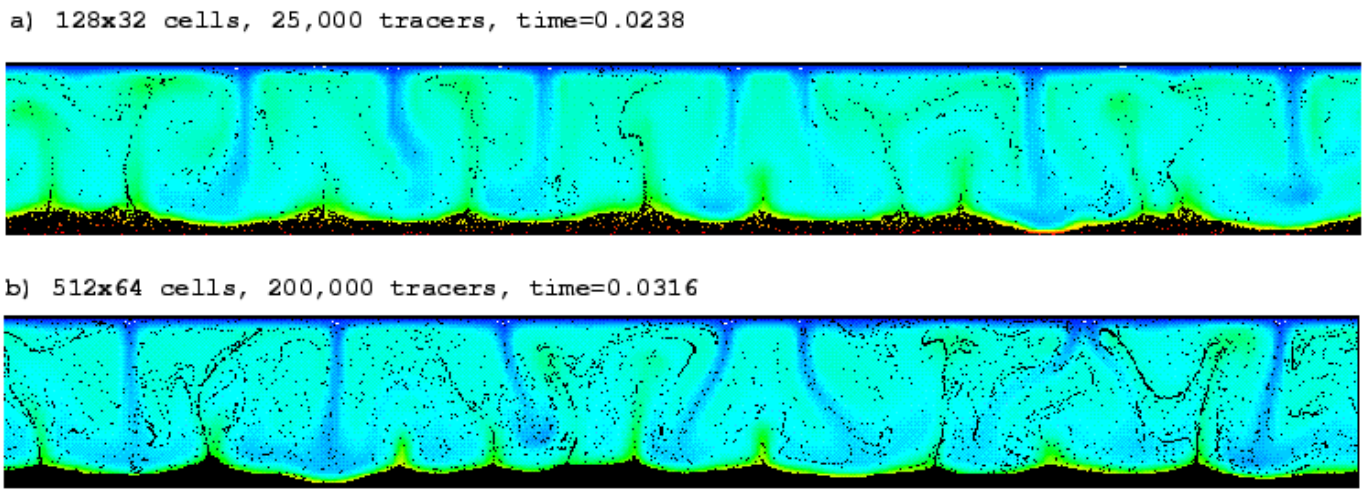

Plate 1. The effect of numerical resolution on the convection pattern: the two-dimensional, Boussinesq case with B=1.0, calculated with two different resolutions and number of tracer particles. (a) 128 by 32 cells, 25000 tracers, time=0.0238, and (b) 512 by 64 cells, 200,000 tracers, time=0.0316. The convection patterns look qualitatively identical, even though there are large quantitative differences in the rate of entrainment.

with the top boundary isothermal and the bottom boundary either isothermal (basally-heated cases) or insulating (completely internally-heated cases). For each combination of thermodynamic and heating parameters, an isochemical case (i.e., with no dense chemical layer) was run until it reached statistically steady-state; this provided the temperature field for initializing chemically-layered cases. The chemical field was initialized with a dense chemical layer of thickness 0.1 (290 km) at the base of the mantle. Simulations were run until the system had adjusted to the presence of the dense layer, or in many cases, until the layer was completely entrained. The simulation time was typically in the range 0.03-0.07 nondimensional time units (scaling to real time is discussed later), requiring 10-20,000 numerical time steps.

Three sets of cases were performed: (i) Boussinesq, constant properties, no phase transitions. (ii) Compressible, depth-dependent viscosity and other properties, with phase transitions. (iii) As (ii), with a viscosity that is dependent on temperature as well as depth. Experiments were heated either 100% from below, or 100% from within, in order to elucidate the basic physics associated with the different heating modes. The radiogenic heating rate for the internally-heated cases was chosen to give the same surface heat flow as the equivalent isochemical basally-heated case. This allows the same temperature scale to be used for all cases, which is important when temperature-dependent viscosity and phase changes are included. For each set, a suite of 2-D calculations with varying chemical buoyancy ratio B were performed. A subset of the cases were then run in 3-D.

RESULTS

The simulations performed are summarized in Table 3. The 3-D cases were chosen to be the ones with the smallest B for which the dense layer survived for a significant length of time, i.e., a reduction of B by a factor of 2 would result in rapid overturn and mixing of the dense layer, as seen in [*Olson and Kincaid*, 1991]. For reasons of length this paper will focus only on six 3-D cases, one for each parameter combination. R.m.s. surface velocities (Table 3) all scale to less than 1 cm/year using the conversions listed in Tables 1 and 2, suggesting that the Rayleigh number should be increased by an order of magnitude to reach the Earth-like parameter range, although a smaller increase is indicated by the heat fluxes. The low surface velocities also affect the scaling of times to dimensional values: a conversion based simply on thermal diffusion timescales (as in Tables 1 and 2) would lead to run times in the range 10-30 Gyr, numbers which should perhaps be reduced by a factor of 5 to reflect the lower than Earth-like velocities.

Boussinesq Cases

Plate 2 shows the time evolution of the basally-heated case with B=1.0, showing the initial state, a time when the system has adjusted to the presence of the layer, and a later time when the layer has been mostly entrained. Plate 3 shows the initial state and a well-adjusted state for the internally-heated case. The presence of the dense layer clearly has substantial effects on the pattern of convection and on the temperature distribution, in addition to displaying its own interesting dynamics.

Thermal planform. The chemically-stable layer at the base of the mantle changes the planform and horizontal lengthscales of the convection, dramatically so in the basally-heated case. In that case, the planform changes from one characterized by upwelling and downwelling sheets (for isochemical convection), to one dominated by upwelling and downwelling plumes. In addition, the horizontal lengthscale has become much smaller, i.e., the upwellings and downwellings are now much more closely spaced. This can be understood by considering that due to the dense stable layer, the 'effective' lower boundary condition for the upper ~0.9 of the mantle has changed from being free-slip to rigid: the convective pattern observed is thus characteristic of rigid-lid convection [*Tackley*, 1993; *Ratcliff et al.*, 1997]. In internally-heated convection, the dynamics are dominated by the upper boundary layer; the lower boundary condition does not have much effect, and so the effect on planform is much lower, although still noticeable.

Chemical structure and entrainment. In both cases the dense chemical material is thinned under downwellings and thickened under upwellings, such that the thick regions form an interconnected series of ridges. This pattern is commonly known as the spoke pattern in thermal convection experiments, and has apparently also been observed in laboratory experiments with a dense chemical layer [*U.R. Christensen, personal communication*]. Entrainment of the layer occurs in

Table 3. Simulations performed.

Formulation	F	$v_{surf,\ rms}$	Phase Buoyancy Parameter P						
			0.03125	0.0625	0.125	0.25	0.5	1.0	2.0
Bouss, B	19.4	910					•	•	◊
Bouss, I	19.4	280				◊	•	◊	◊
Compr, B	17.5	1150				◊	•	◊	
Compr, I	18.0	870			◊	•	◊		
C+η(T), B	15.8	620		◊	◊	•	◊		
C+η(T), I	18.0	750	◊	◊	•	◊			

'◊ ' indicates a 2-D simulation only, '•' indicates both 3-D and 2-D simulations, 'B' means basally-heated, 'I' means internally-heated, F is the heat flux, and $v_{surf,rms}$ is the rms. surface velocity.

cylindrical plumes which form at the intersection of these ridges. Plate 4 shows a zoomed-in view of the chemical and thermal fields for the two cases, highlighting this cylindrical entrainment.

It is perhaps surprising that internally-heated system also displays cylindrical entrainment. In a 100% internally-heated system, there are no active upwellings: the downwellings are usually cylindrical and the upwelling is in the form of a general distributed return flow. Despite this lack of active upwellings, the chemical field displays very similar dynamics, forming a spoke pattern and cylindrical entrainment plumes. One effect which may be partly responsible for this is that the lower layer heats up, due to radiogenic heat sources and the inability of this volumetric heating to escape by means other than rather slow thermal conduction, and may thus become a heat source for active upwellings. How rapid is this heating up? The chondritic abundance of heat-producing elements would cause a temperature rise of 136 K per billion years, based on current radioactive decay rates. Although this rate is small, it may be important if the layer can survive for the age of the Earth, particularly since the rate of heat production was higher in the past.

The rate of entrainment is much lower in the 100% in-

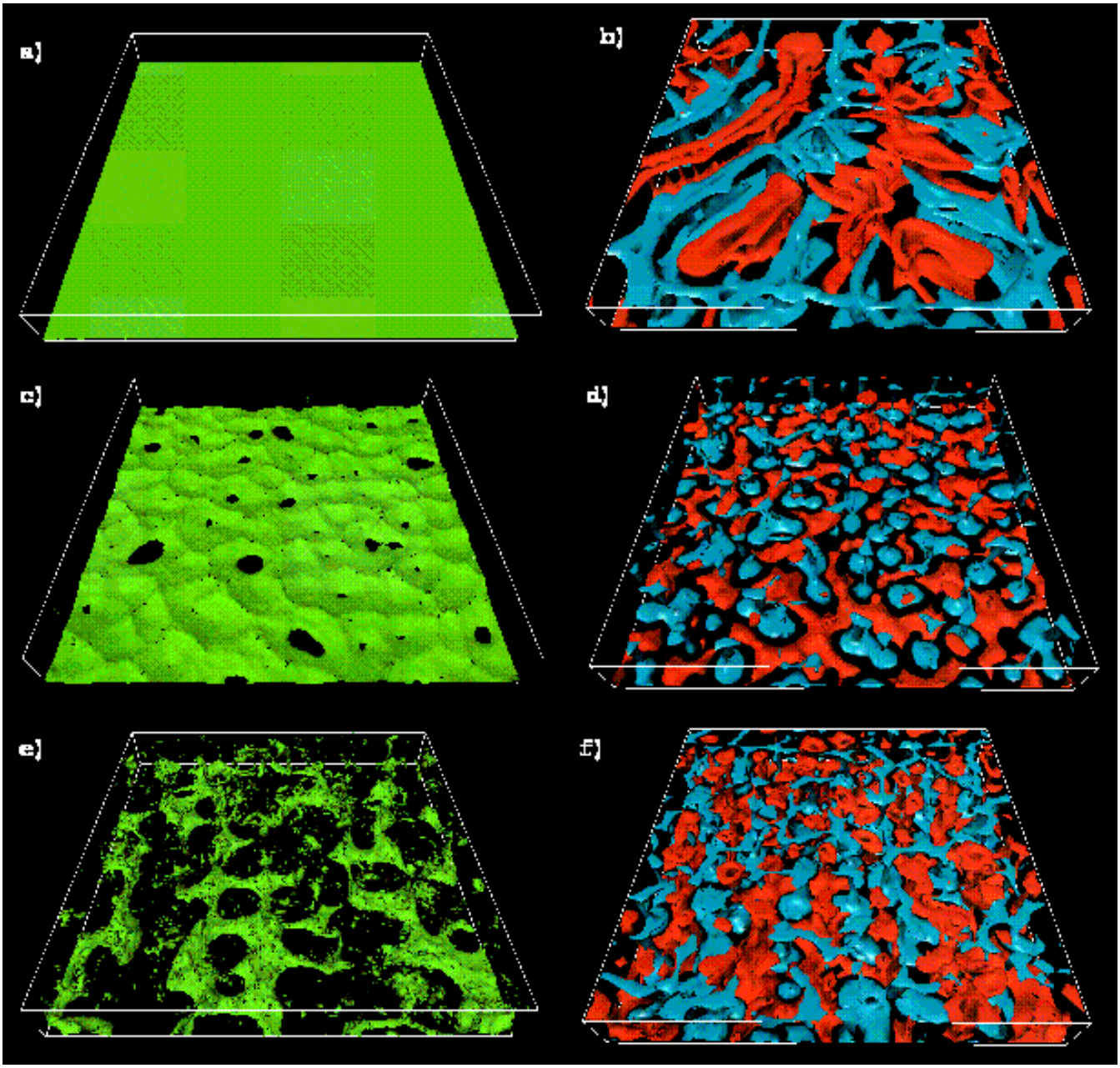

Plate 2. Boussinesq, basally-heated case with B=1.0 at three different times. The left parts (a., c., and e.) show an isocontour of the compositional field, corresponding to C=0.3, and the right parts (b., d., and f.) show isosurfaces of the residual temperature field, showing where the temperature is 0.1 hotter (red) or 0.1 colder (blue) than the horizontal average. The times are t=0 (a. and b.), t=0.0345 (c. and d.) and t=0.0693 (e. and f.).

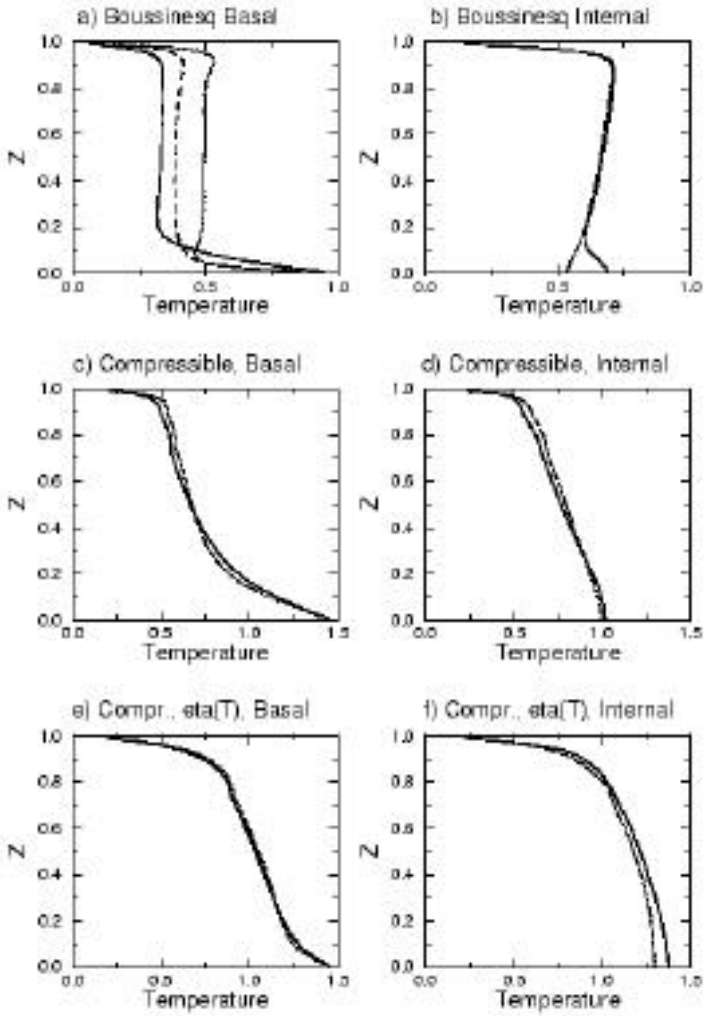

Figure 3. Temperature profiles (geotherms) for the six 3-D cases reported. Dotted lines indicate initial temperature profiles (i.e., for isochemical cases), whereas solid lines indicates the temperature profiles for the times illustrated in the Figures 4, 5, 8 and 10. For the Boussinesq, basal case, an additional dashed line shows the profile for the third time illustrated in Plate 2.

ternally-heated cases than in the 100% basally-heated cases, for the same buoyancy parameter B. For example, with B=0.5, the dense layer experiences rapid overturn and mixing for basal heating, but is stable and survives for a long time with 100% internal heating. This is not surprising since there are no active upwellings to entrain the dense material. In addition, the temperature drop across the mantle, ΔT, is lower in the internally-heated case even though surface heat flow is the same: if this lower ΔT were used in the calculation of B, a larger B would result. If ΔT over the chemical layer were used instead of total ΔT, an even larger difference would be found. At first glance this finding would appear to be at odds with [*Christensen and Hofmann*, 1994], who found that the fraction of internal heating did not affect the rate of entrainment of a dense layer. The main differences are probably that all their cases included mixed heating from below and within so that active upwellings always existed, and that the internal heating was varied over a smaller parameter range. When basal heating is switched off altogether, entrainment of the layer is considerably slower.

Temperature profiles. The dense layer also has a strong effect on the horizontally-averaged temperature profile (geotherm), as illustrated in Figure 3, which compares temperature profiles for isochemical and layered cases. With basal heating (Figure 3(a)), the dense layer acts as a thermal blanket over the core, reducing the interior temperature by up to 0.17 (nominally 425 K), and increasing the temperature drop over the lower thermal boundary layer by a corresponding amount. This larger ΔT results in stronger upwellings which are able to entrain the dense layer more effectively. Thus, the rate of entrainment increases as time goes on. At a later time (dashed line) the layer has been substantially entrained, the thermal blanketing is lower, and the internal temperature is rising again.

With pure internal heating (Figure 3(b)), the effect on internal temperature is minimal, but a new region of high temperatures is observed in the dense layer. This is due to trapped radiogenically-produced heat, as discussed above, and results in horizontally-averaged temperature anomalies of up to 0.16 (nominally 400K). The internal temperature profile is subadiabatic, as expected for substantially internally-heated convection [*Schubert*, 1992; *Parmentier et al.*, 1994; *Tackley*, 1996].

Compressible, Depth-Dependent Properties

Structures. The thermal and compositional fields for basally- and internally-heated cases at times when the system has adjusted to the presence of the dense layer are shown in Plate 5. Initial temperature distributions are not shown because they look very similar to the illustrated temperature distributions, except for features being somewhat narrower in the deep mantle. The convective planforms are very stable and the long wavelength structure does not change much with time, as is characteristic for convection with strongly depth-dependent properties [*Balachandar et al.*, 1992; *Hansen et al.*, 1993; *Zhang and Yuen*, 1995; *Bunge et al.*, 1996]. The phase transitions do not appear to be having much effect on the convection, probably due to the viscosity increase at 660 km depth [*Monnereau and Rabinowicz*, 1996; *Bunge et al.*, 1996].

In contrast to the Boussinesq, constant-property cases, (i) the dense material does not have a large effect on the thermal structure, and (ii) the dense material is swept into very large piles (or ridges in the internally-heated case), which extend vertically most of the way through the lower mantle. These two effects are no doubt related: since the dense material is swept into discrete piles it no longer acts as a thermal blanket over the core, and it no longer acts as an effectively rigid boundary condition on the flow above.

Large topography. Why does the dense material form large, thick piles instead of a continuous, varying-thickness

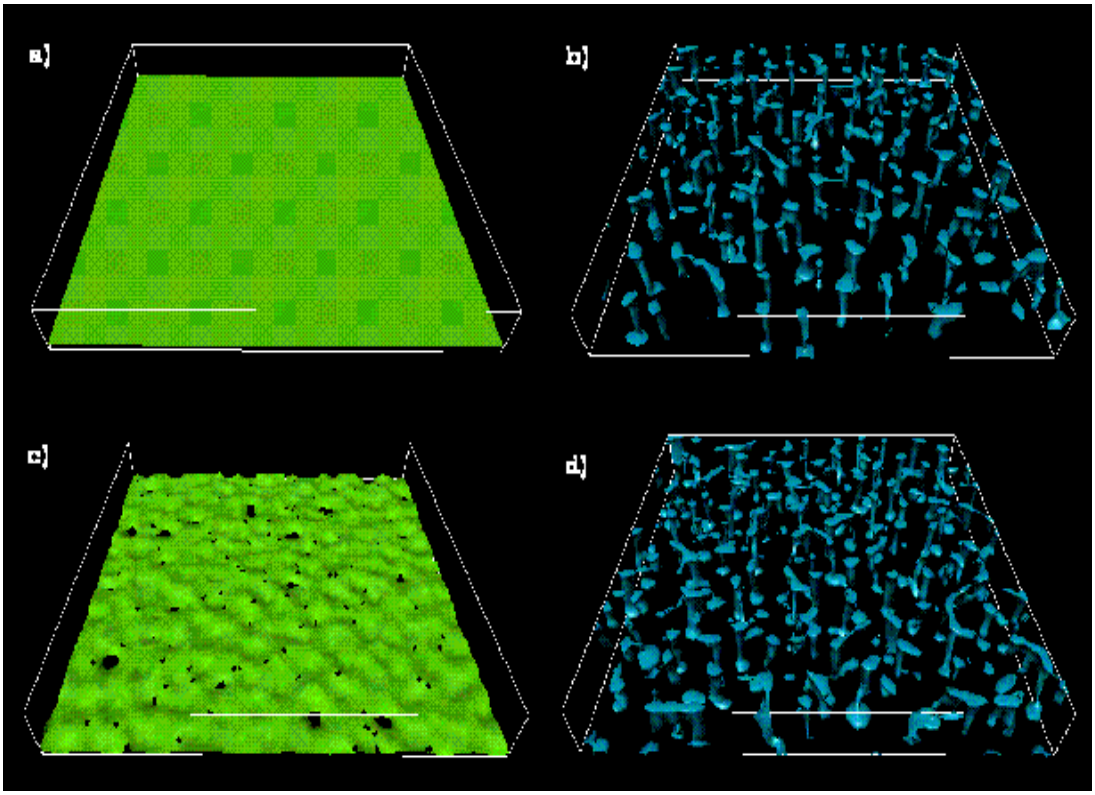

Plate 3. Boussinesq, internally-heated case with B=0.5 at two different times: the initial state (a. and b.), and t=0.0463 (c. and d.). Compositional isocontour C=0.3 (a. and c.), and residual temperature isocontour t=-0.1 (b. and d.).

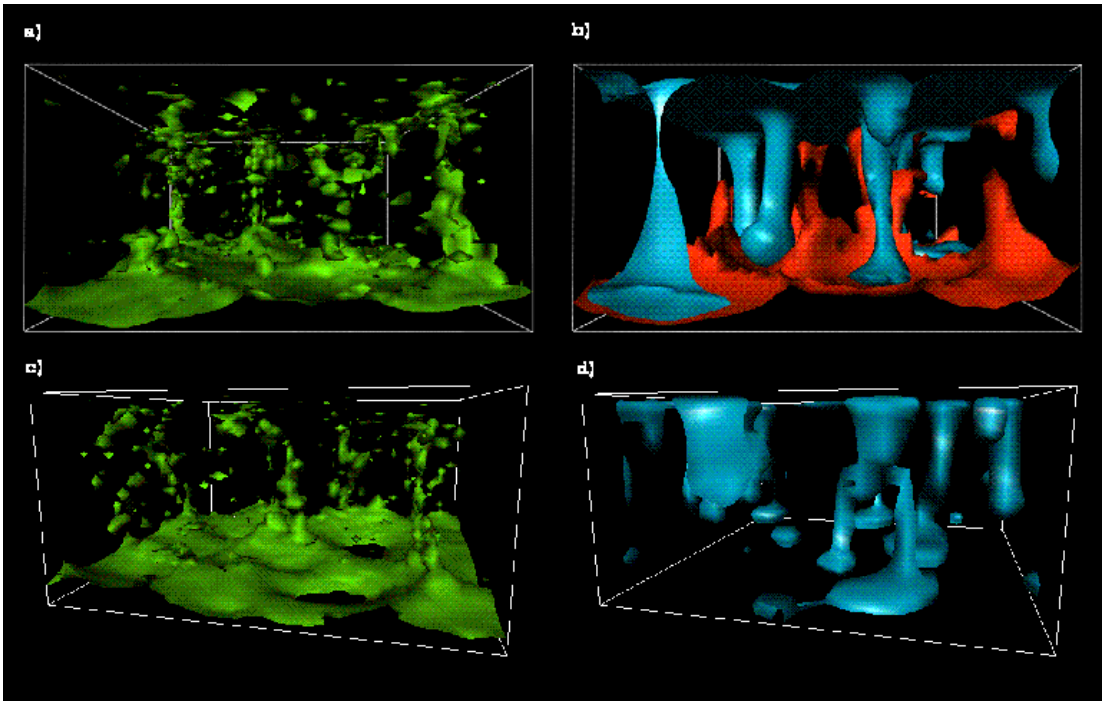

Plate 4. Zoom in views of the Boussinesq basally-heated case (top) and internally-heated case (bottom) showing cylindrical entrainment features. Composition isocontour C=0.08 (a.) and C=0.1 (c.). Residual temperature isocontours are T=0.1 (red) and T=-0.1 (blue).

layer as in the constant-property cases? An obvious explanation might be that the buoyancy parameters B_{surf} are lower in these cases, at 0.5 and 0.25 compared to 1.0 and 0.5, which would allow thermal buoyancy to lift the material further. However, it is probably more appropriate to calculate B using the density and thermal expansivity near the CMB, since this is where the dense material resides. This results in B_{cmb} of 1.5 and 0.75, actually larger than the constant properties cases. The main reason for the increased topography is the low local Rayleigh number

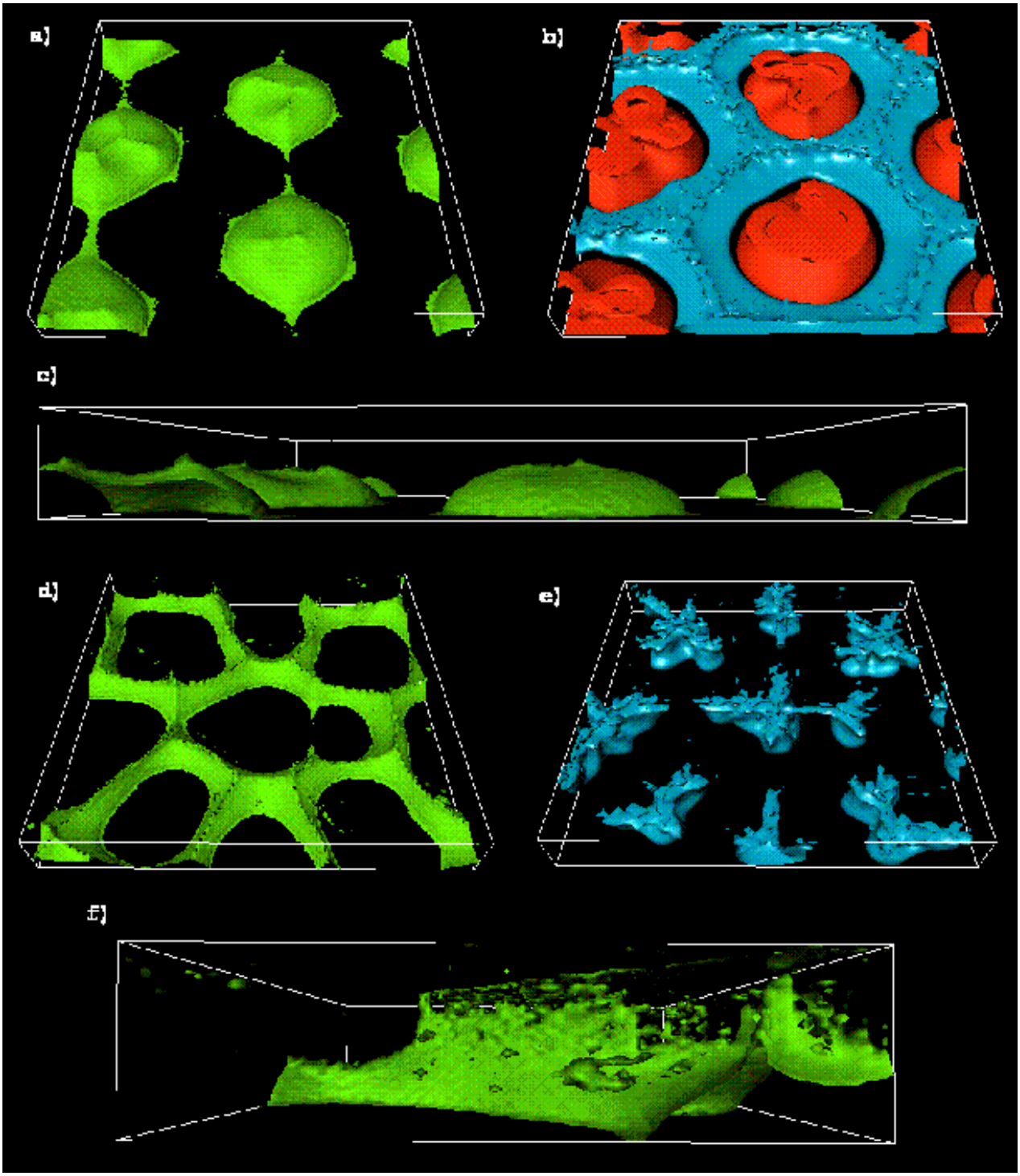

Plate 5. Compressible, depth-dependent viscosity cases. (a.-c.) Basally-heated, B_{surf}=0.5 (B_{cmb}=1.5), time=0.023, and (d.-f.) internally-heated, B_{surf}=0.25 (B_{cmb}=0.75), time=0.026. Compositional isocontour C=0.3 (green, a., c., d., and f.) and residual temperature isocontours 0.1 (red) and -0.1 (blue).

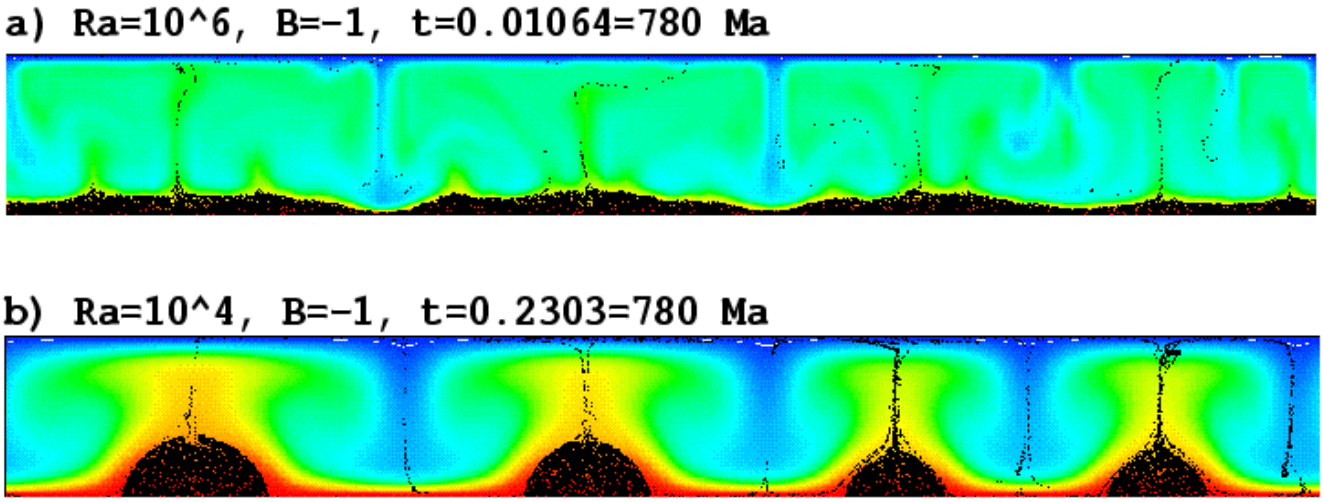

Plate 6. Effect of Rayleigh number on the topography of the dense layer, for two-dimensional, basally-heated Boussinesq cases with B=0.1. (a) Ra=10^6, t=0.0106, (b) Ra=10^4, t=0.2303. Note that when scaled by the velocities, these two times are almost identical.

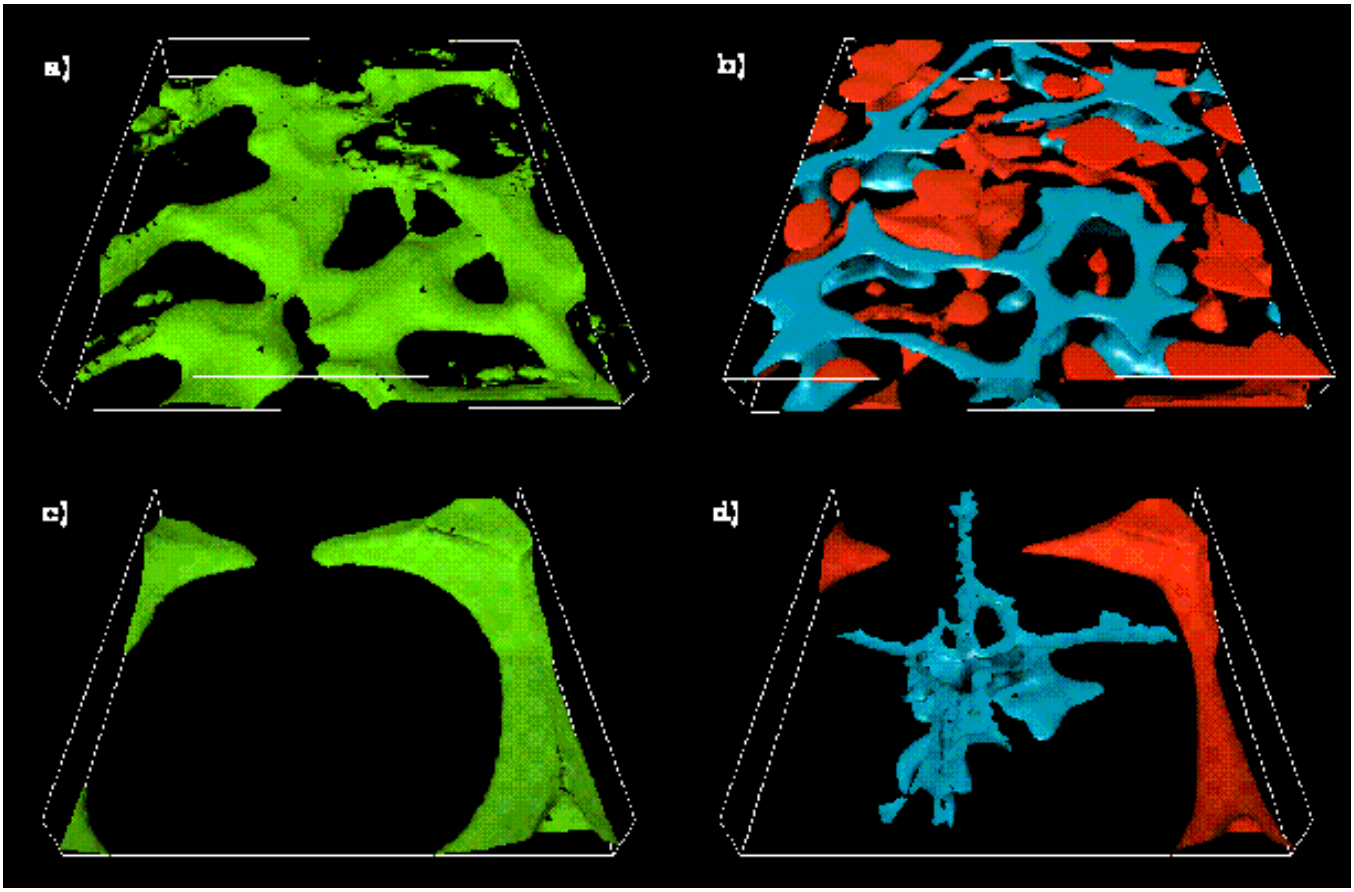

Plate 7. Compressible, temperature- and depth-dependent viscosity cases. (a.-b.) Basally-heated, B_{surf}=0.25 (B_{cmb}=0.75), time=0.0321, and (c.-d.) internally-heated, B_{surf}=0.125 (B_{cmb}=0.375), time=0.0367. Compositional isocontour C=0.3 (green, a. & c.) and residual temperature isocontours 0.1 (red) and -0.1 (blue).

in the deep mantle (Ra_{cmb}=4x10^3) due to depth-dependent viscosity, thermal diffusivity, and thermal expansivity. The effect of *Ra* on dense layer topography is illustrated in Plate 6, for a two-dimensional, constant-properties scenario with B=1.0. At Ra=10^6, a continuous, varying-thickness layer is formed, but at Ra=10^4, discrete piles are formed, somewhat similar to the piles in the 3-D compressible cases. The reason for this increased topography is the increased stresses associated with the thicker upwellings and downwellings in the lower *Ra* case. (Note that with the conventional thermal nondimensionalization, nondimensional stresses *increase* with increasing *Ra*, even though *dimensional* stresses decrease with increasing Ra). If the stress scaled as the thickness of the upwellings and downwellings, i.e., approximately $Ra^{-1/3}$, this would predict ~4.5 times as much topography in the lower *Ra* case, which appears to be an upper bound on what is observed.

Temperature profile. As with the three-dimensional structure, the dense material does not have a large effect on the horizontally-averaged temperature (Figure 3(c) and (d)). The lower boundary layer in the basally-heated case extends over the lower ~0.25 (700 km) of the mantle, rather larger than commonly assumed, but consistent with previous calculations of convection with reasonable depth-dependent properties [*Balachandar et al.*, 1992; *Tackley*, 1996].

Temperature-Dependent Viscosity

Structures. Thermal and compositional fields for basally- and internally-heated cases at times when the system has adjusted to the presence of the dense layer are shown in Plate 7. As with the depth-dependent viscosity cases, large piles of dense material are formed, and the dense material does not have a huge effect on overall large-scale thermal structure.

The buoyancy parameters needed to get long-term stability are reduced by a factor of two compared to the depth-dependent viscosity cases, at B_{surf}=0.25 (B_{cmb}=0.75) and B_{surf}=0.125 (B_{cmb}=0.375). The two main reasons for this are probably (i) due to the high viscosity upper boundary layer the interior temperature is higher, reducing the temperature drop over the CMB boundary layer, hence the thermal buoyancy available for upwellings to entrain the dense material, and (ii) due to the temperature-dependence of viscosity, the dense material is less viscous than the mantle above, and thus more difficult to entrain [*Kellogg and King*, 1993]. It has also been suggested that dense D" material may be more viscous than the mantle above, also making it more difficult to entrain [*Manga*, 1996]. However, any intrinsic compositional effects are likely to be overwhelmed by the very strong dependence of viscosity on temperature [*Sleep*, 1988].

The internally-heated planform perhaps now looks the more 'Earth-like' of the two, with long-wavelength structure and chemical structure that is dominated by a single pile with ridge-like extension. The chemical pile has heated up due to the radiogenic heat sources, and results in a hot temperature structure which closely mimics the chemical structure. The density effects of the thermal and composition fields largely cancel out.

The temperature profile (Figure 3 (e) and (f)) is again little changed by the chemical field, the main effect being an increase in temperatures in the internally-heated case, presumably due to the inhibiting effect of the dense material on thermal convection, particularly within the dense pile.

Spectral Heterogeneity Maps

A useful tool for making statistical comparisons between convection models and seismic tomographic models is the Spectral Heterogeneity Map (SHM), first introduced by [*Tackley et al.*, 1994]. These show the lateral spectrum of a field (e.g., temperature or seismic velocity) as a function of depth, in the form of a contour plot. SHMs for four of the 3-D cases presented are shown in Figures 4 and 5. The 'spatial frequency', plotted on the horizontal axis, is simply the inverse wavelength

$$sf = 1/\lambda \qquad (15)$$

such that the fundamental mode of the 8x8x1 box has a spatial frequency of 0.125, and a spatial frequency of 1 corresponds to a wavelength of ~3000 km, corresponding roughly to spherical harmonic L=13.

These figures show the thermal and compositional fields, and also the total density anomaly field, which is a combination of the two, given by:

$$\rho = \bar{\alpha}\bar{\rho}.T - B_s.C \qquad (16)$$

It would also be interesting to plot the seismic velocity field, for direct comparison with seismic tomography. However, the scaling factor between temperature and seismic velocity is somewhat uncertain in the deep mantle, and the scaling factor between composition and seismic velocity is arbitrary since we have not assigned any particular composition to this field.

The Boussinesq, basally-heated, isochemical case (Figure 4 (a)) has a strong (and equal) concentration of heterogeneity in the upper and lower thermal boundary layers, with little in-between, as is normal for this configuration [*Jarvis and Peltier*, 1986]. Adding the dense chemical layer (part (c)) results in much more heterogeneity in the lower TBL than in the upper one, and shifts the peak to shorter wavelengths (higher spatial frequency). The chemical field (part (e)) displays strong heterogeneity at the base of the mantle, as expected. The density field (part (g)) displays heterogeneity in both the upper and lower boundary layers, with the lower boundary layer being somewhat stronger.

Two interesting points arise from the above plots. (i) The vertical extent of D" density heterogeneity is less than that of either chemical or thermal heterogeneity, i.e., estimating the thickness of D" from the density field would

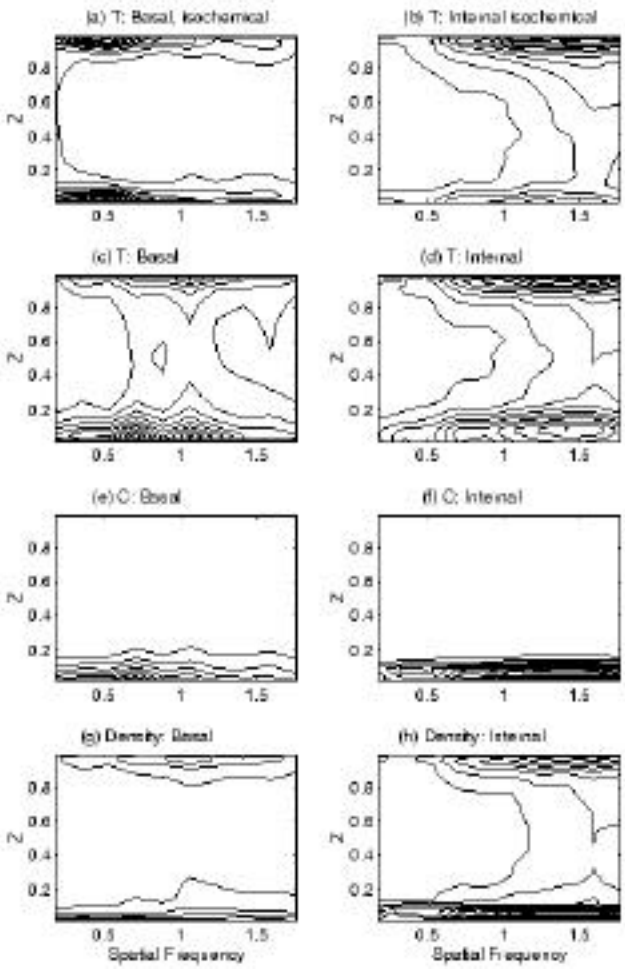

Figure 4. Spectral heterogeneity maps (i.e., contour plots of the rms. amplitude of heterogeneity as a function of depth and horizontal spatial frequency) for the Boussinesq cases. (a., c., e., and g) basally-heated case, and (b., d., f., and h.) internally-heated case. (a. and b.) show the initial temperature field (for isochemical convection), the other parts show fields for the times illustrated previously: (c. and d.) temperature field, (e. and f.) chemical field, (g. and h.) total density. A spatial frequency of 1 is roughly equivalent to spherical harmonic degree 13.

result in a smaller estimate than by using the thermal or compositional field individually. This is because the system arranges itself in such a way that thermal and compositional densities tend to cancel each other out, particularly near the top of the compositional layer. (ii) Whereas temperature heterogeneity is zero right at the CMB (because of the isothermal boundary condition in basally-heated cases), compositional heterogeneity reaches a peak at this depth. This could, in principle, be used as a way of distinguishing thermal from compositional heterogeneity near the base of D".

The internally-heated Boussinesq case displays similar trends to the basally-heated case, except that the dominant heterogeneity is shorter-wavelength and is less affected by the dense layer, and the thermal heterogeneity does not go

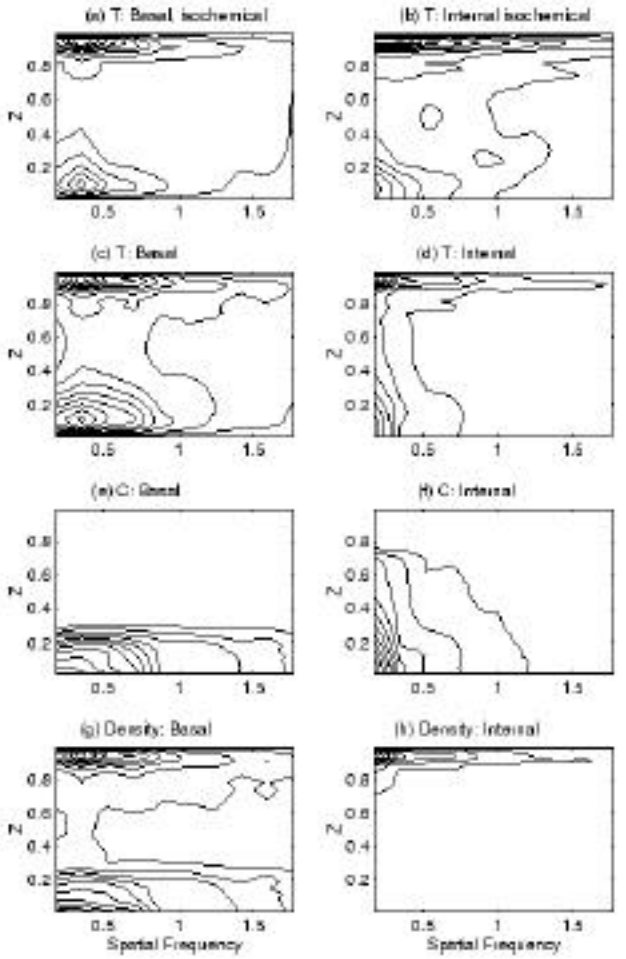

Figure 5. As Figure 4 but for compressible, depth- and temperature-dependent viscosity cases.

to zero at the CMB because the boundary condition is zero flux rather than isothermal. An isothermal boundary condition is more realistic for the Earth, however, so point (ii) above still stands.

Due to length limitations, only the compressible, temperature-dependent viscosity cases are shown (Figure 5). In both cases, long-wavelength heterogeneity dominates. In the basally-heated result (left column), the heterogeneity associated with the lower TBL now extends through a large fraction of the lower mantle, consistent with the geotherm plot (Figure 3(e)), and is slightly increased by the addition of the dense material. The chemical heterogeneity also extends to mid way through the lower mantle, but density heterogeneity is more confined due to the cancellation of thermal and chemical buoyancy in the mid-mantle. The internally-heated case displays the same trends, with cancelation of thermal and chemical buoyancy effects so effective that the signature of the dense layer is lost in the density SHM. The compressible cases with depth-dependent viscosity (not illustrated here) have similar SHM except that the upper boundary layer has a lower amplitude.

The compressible cases all display an abrupt change in the amplitude of heterogeneity and of the lateral spectrum at mid-lower-mantle depth. This is compatible with seismic tomographic models, for example [*Su et al.*, 1994], which also display an increase in amplitude and reddening of the spectrum at this depth [*Tackley et al.*, 1994; *Schubert and Tackley*, 1995].

DISCUSSION

Thermo-Chemical Stationary Megaplumes

The compressible simulations display large piles of material which extend much of the way through the lower mantle and can survive over geological time. For example, the internally-heated, temperature-dependent-viscosity case is illustrated in Plate 7 at a time of 0.0367 (which corresponds to somewhere between 1 and 13 Gyr depending on whether the r.m.s. surface velocity or thermal diffusion is used for the dimensional scaling), and shows very little entrainment. "Megaplumes" which may be compatible with these structures are observed under Africa and the Pacific in global seismic tomographic models [*Su et al.*, 1994; *Masters et al.*, 1996; *Grand et al.*, 1997; *van der Hilst et al.*, 1997]. These megaplumes extend vertically at least half way through the lower mantle but then appear to stop, with no obvious low-velocity vertical continuation through the rest of the mantle, a surprising behavior if they are interpreted purely as hot thermal structures, which should rise without inhibition throughout the mantle, perhaps thinning as they rise due to decreasing viscosity. The present results suggest that megaplumes may be both chemical and thermal in origin, with their topography maintained by a balance between positive thermal buoyancy and negative chemical buoyancy, thus explaining why they do not move upwards. Internal circulation occurs within the megaplumes, and they may heat up due to radiogenic heat trapped over geological time, as well as heat conducted through the CMB. The regions above these megaplumes appear to be preferential locations for hotspots. In the proposed scenario, plumes would arise off the top of these megaplumes and might entrain some of the chemically anomalous material.

In addition to (i) the apparent stationarity of the megaplumes discussed above, this thermo-chemical hypothesis might also explain: (ii) The location of a geochemical reservoir, perhaps the high-$^3He/^4He$ reservoir, and perhaps containing the heat-producing elements which appear to be missing in the MORB source. The material is slowly entrained from its top by 'hotspot' plumes and/or the background mantle flow. (iii) The large variation of seismic velocities in the deep mantle, apparently too large to be explained purely by thermal effects [*Wysession*, 1996], an observation which has already led to the inference of chemical variations [*Yuen et al.*, 1993; *Cadek et al.*, 1994; *Yuen et al.*, 1996]. (iv) The breakdown in scaling between shear and compressional velocities in the deep mantle [*Bolton and Masters*, 1996; *Robertson and Woodhouse*, 1996]. The main breakdown appears localized to a region under the Pacific [*Bolton and Masters*, 1996], the location of a 'megaplume'. (v) The change in character of seismic heterogeneity at mid-lower-mantle depths, as seen by a change in lateral spectrum [*Tackley et al.*, 1994] and a broadening of the radial correlation function [*Jordan et al.*, 1993]. (vi) The best fit to the geoid is obtained when the only buoyancy forces are provided by downwelling slabs [*Ricard et al.*, 1993], suggesting that slow regions may be neutrally buoyant.

Density Contrast Required for Stable Layering

While the present study does not attempt to closely define the transition from rapid overturn to stable layering (taking Buoyancy ratios that are separated by a factor of two), it is useful to consider what constrains it does place on the required density contrast. The density contrasts associated with various Buoyancy ratios for Boussinesq and compressible scenarios are listed in Table 4.

For the Boussinesq cases, the answer depends proportionally on what the average mantle thermal expansivity is taken to be, and on what temperature drop is assumed. For the values listed in Table 1, the results indicate that for basal heating a density contrast of 6.25% results in stable layering, whereas a density contrast of 3.125% results in rapid overturn.

Internal heating reduces the required density contrast, as does compressibility (mainly because of the decrease of thermal expansivity with depth), and temperature-dependent viscosity. For the case with all three of these components, a density contrast of only 0.94% of CMB density, or 1.56% of surface density, is sufficient for long-term stability of the chemical layer.

Table 4.Equivalent density contrasts for buoyancy ratios *B*

B_{surf}	Boussinesq		Compressible			
	$\Delta\rho$ (kg/m^3)	$\Delta\rho$ (%)	$\Delta\rho$ (kg/m^3)	$\Delta\rho/\rho_{surf}$ (%)	$\Delta\rho/\rho_{cmb}$ (%)	B_{cmb}
1.0	250	6.25	412.5	12.5	7.5	3.0
0.5	125	3.125	206.25	6.25	3.75	1.5
0.25	62.5	1.562	103.125	3.125	1.875	0.75
0.125	31.25	0.781	51.5625	1.5625	0.9375	0.375

How 'long-term' is the layer's stability? [*Sleep*, 1988] calculates analytically that a 6% density contrast is required for the layer to remain over the age of the Earth, assuming $\alpha=2x10^{-5}$. This would reduce to 3% if a more realistic deep-mantle α of $1x10^{-5}$ were used. The numerical results in this present study, which may substantially overestimate the entrainment rate (see earlier discussion) suggest that a dense layer can survive over geological timescales with a smaller density contrast than this, although this needs to be more specifically and accurately addressed in the future. The density contrast also affects the topography on the top of the layer: lower density contrasts result in larger topography.

CONCLUSIONS

Simple 3-D Boussinesq, constant-properties simulations of mantle convection with a preexisting dense chemical layer at the base indicate that, if the dense layer has a sufficient density contrast to be stable for long periods (i.e., ~5% or more): (i) the layer forms a spoke pattern, with an interconnected network of ridges, (ii) entrainment occurs in cylindrical plumes rising from the intersections of these ridges, even in 100% internally-heated cases, (iii) the layer heats up even with zero basal heat flux because of trapped radiogenically-produced heat, (iv) thermal blanketing of the core reduces the interior mantle temperature, (v) the layer acts as an effective rigid lower boundary condition, reducing the horizontal lengthscales of the thermal convection, and (vi) internal heating reduces the ability of the thermal convection to entrain the layer.

With depth-dependent viscosity and other properties included within the framework of a compressible formulation, (i) the density contrast required for long-term stable layering is reduced, and (ii) material may be swept into large, thermo-chemical megaplumes extending ~half way through the lower mantle. Temperature-dependent viscosity further reduces the density contrast required for stable layering.

Examination of the depth variation of thermal, compositional, and density heterogeneity, and the lateral spectrum of heterogeneity at different depths using spectral heterogeneity maps (SHMs) indicates that (i) the dense layer increases the lateral heterogeneity of thermal and total density fields in the deep mantle, (ii) thermal and compositional buoyancy (density) contributions cancel out in the upper part of the dense layer, (iii) while thermal heterogeneity is zero at the CMB due to the isothermal boundary condition, chemical heterogeneity peaks, providing a potential means of distinguishing the two, and (iv) for the compressible cases a dramatic change in the lateral heterogeneity takes place at depths corresponding to the top of the thermo-chemical megaplumes. This change in heterogeneity is also apparent in seismic topographic models.

The thermo-chemical megaplumes may provide an explanation for various geophysical observations as discussed earlier, but do not explain D", since (i) the discontinuity topography (where it is observed) varies by much less, from ~150 to ~450 km; and (ii) the discontinuity is still observed under inferred mantle downwellings [*Kendall and Shearer*, 1994], incompatible with numerical results where it is swept completely aside. Smaller topography could be recovered by increasing the density contrast. However, mineralogical constraints [*Sidorin and Gurnis*, 1998] indicate that large density contrasts are physically implausible. Another possibility that would reduce the topography is that the viscosity in the deep mantle is lower than assumed here (hence the local Rayleigh number is higher), due to a smaller increase with depth or a lower near-surface "reference" value. This is quite possible since the deep mantle viscosity is not well constrained by postglacial rebound or geoid modeling approaches.

Thus, there are various difficulties with explaining D" in terms of a thermo-chemical boundary layer. Firstly, as discussed above, with a small, mineralogically-feasible density contrast and high deep-mantle viscosity, the topography generated on the top of the layer will be much larger than seismically observed. Even if reasonable density and topography are possible, there some difficulties which center around obtaining a sharp seismic reflection while simultaneously generating heterogeneity down to small lengthscales. If the layer were primordial, it might be able to preserve a fairly sharp boundary over geological time (if the layer survives at all [*Sleep*, 1988]), but short-wavelength lateral variations would be difficult to generate since the lateral variations tend to have the same scale as the driving thermal field, as illustrated by the presented calculations. If, on the other hand, the layer were dynamically generated through the segregation of oceanic crust or reactions with the core, short-scale lateral variations are expected but the transition from the dense material to normal mantle is probably too gradual [*Kellogg and King*, 1993; *Christensen and Hofmann*, 1994] to generate a seismic reflection.

The true situation is probably more complicated than can be modeled with a single compositional field. For example, D" could be partly primordial and partly dynamically-generated, resulting in a complex interplay of compositional and thermal effects, although the density problem still exists. One appealing possibility is that the seismic discontinuity is unrelated to chemistry but is generated by a phase transition [*Stixrude and Bukowinski*, 1990; *Nataf and Houard*, 1993]. This is particularly appealing since it allows the existence of thermo-chemical megaplumes to explain various geophysical observations, in addition to the "Lay discontinuity".

Future work must address these problems and possibilities in detail, and determine what seismic signatures are produced from various dynamically-produced thermo-chemical structures. The detailed dynamics of potential slab segregation at the CMB [*Olson and Kincaid*, 1991] and the fate of the two differentiated components needs further evaluation, as does the question of long-term survivability of a dense layer for geophysically reasonable density contrasts and other parameters. A greater understanding of the relevant mineral physics, including the possible existence of a phase transition, will clearly also play an essential role.

Acknowledgments. Simulations were performed on the Intel Paragon and Cray T3E at San Diego Supercomputer Center and the Cray T3E at NASA Goddard Space Flight Center. Supported by NSF, NASA and IGPP/LANL.

REFERENCES

Anderson, D.L., A seismic equation of state .2. Shear properties and thermodynamics of the lower mantle, *Phys. Earth Planet. Inter.*, *45*, 307-323, 1987.

Anderson, O.L., H. Oda, and D. Isaak, A model for the computation of thermal expansivity at high compression and high temperatures - MgO as an example, *Geophys. Res. Lett.*, *19*, 1987-1990, 1992.

Balachandar, S., D.A. Yuen, and D. Reuteler, Time-dependent 3-dimensional compressible convection with depth-dependent properties, *Geophys. Res. Lett.*, *19*, 2247-2250, 1992.

Bolton, H., and G. Masters, A region of anomalous dlnVs/dlnVp in the deep mantle, *Eos Trans. AGU, Fall Meeting Suppl.*, *77*, 697, 1996.

Brandt, A., Guide to multigrid development, *Lecture Notes In Mathematics*, *960*, 220-312, 1982.

Bunge, H.P., M.A. Richards, and J.R. Baumgardner, Effect of depth-dependent viscosity on the planform of mantle convection, *Nature*, *379*, 436-438, 1996.

Bunge, H.P., M.A. Richards, and J.R. Baumgardner, A sensitivity study of 3-dimensional spherical mantle convection at 10^8 Rayleigh number - Effects of depth-dependent viscosity, heating mode, and an endothermic phase change, *J. Geophys. Res.*, *102*, 11991-12007, 1997.

Cadek, O., D.A. Yuen, V. Steinbach, A. Chopelas, and C. Matyska, Lower mantle thermal structure deduced from seismic tomography, mineral physics and numerical modeling, *Earth Planet. Sci. Lett.*, *121*, 385-402, 1994.

Chopelas, A., and R. Boehler, Thermal expansivity in the lower mantle, *Geophys. Res. Lett.*, *19*, 1983-1986, 1992.

Christensen, U., Instability of a hot boundary layer and initiation of thermo-chemical plumes, *Annales Geophysicae*, *2*, 311-319, 1984.

Christensen, U.R., Models of mantle convection - one or several layers, *Phil. Trans. R. Soc. London A*, *328*, 417-424, 1989.

Christensen, U.R., and A.W. Hofmann, Segregation of subducted oceanic crust In the convecting mantle, *J. Geophys. Res.*, *99*, 19867-19884, 1994.

Christensen, U.R., and D.A. Yuen, Layered convection induced by phase transitions, *J. Geophys. Res.*, *90*, 291-300, 1985.

Davies, G.F., and M. Gurnis, Interaction of mantle dregs with convection - lateral heterogeneity at the core-mantle boundary, *Geophys. Res. Lett.*, *13*, 1517-1520, 1986.

Duffy, T.S., and T.J. Ahrens, Thermal expansion of mantle and core materials at very high pressures, *Geophys. Res. Lett.*, *20*, 1103-1106, 1993.

Dziewonski, A.M., and D.L. Anderson, Preliminary reference Earth model, *Phys. Earth Planet. Inter.*, *25*, 297-356, 1981.

Garnero, E.J., and D.V. Helmberger, Seismic detection of a thin laterally varying boundary-layer at the base of the mantle beneath the central Pacific, *Geophys. Res. Lett.*, *23*, 977-980, 1996.

Grand, S.P., R.D. van der Hilst, and S. Widiyantoro, Global seismic tomography: A snapshot of convection in the Earth, *GSA Today*, *7*, 1-7, 1997.

Gurnis, M., The effects of chemical density differences on convective mixing in the Earth's mantle, *J. Geophys. Res.*, *91*, 1407-1419, 1986.

Hansen, U., and D.A. Yuen, Numerical simulations of thermal-chemical instabilities at the core mantle boundary, *Nature*, *334*, 237-240, 1988.

Hansen, U., and D.A. Yuen, Dynamical influences from thermal-chemical instabilities at the core-mantle boundary, *Geophys. Res. Lett.*, *16*, 629-632, 1989.

Hansen, U., D.A. Yuen, S.E. Kroening, and T.B. Larsen, Dynamic consequences of depth-dependent thermal expansivity and viscosity on mantle circulations and thermal structure, *Phys. Earth Planet. Inter.*, *77*, 205-223, 1993.

Jarvis, G.T., and D.P. McKenzie, Convection in a compressible fluid with infinite Prandtl number, *J. Fluid Mech.*, *96*, 515-583, 1980.

Jarvis, G.T., and W.R. Peltier, Lateral heterogeneity in the convecting mantle, *J. Geophys. Res.*, *91*, 435-451, 1986.

Jordan, T.H., P. Puster, G.A. Glatzmaier, and P.J. Tackley, Comparisons between seismic Earth structures and mantle flow models based on radial correlation functions, *Science*, *261*, 1427-1431, 1993.

Karato, S., and P. Wu, Rheology of the upper mantle - a synthesis, *Science*, *260*, 771-778, 1993.

Karato, S.I., M.S. Paterson, and J.D. Fitzgerald, Rheology of synthetic olivine aggregates - Influence of grain-size and water, *J. Geophys. Res.*, *91*, 8151-8176, 1986.

Kellogg, L.H., and S.D. King, Effect of mantle plumes on the growth of D" by reaction between the core and mantle, *Geophys. Res. Lett.*, *20*, 379-382, 1993.

Kendall, J.M., and P.M. Shearer, Lateral variations in D" thickness from long-period shear wave data, *J. Geophys. Res.*, *99*, 11575-11590, 1994.

Knittle, E., and R. Jeanloz, Simulating the core-mantle boundary - an experimental study of high-pressure reactions between silicates and liquid iron, *Geophys. Res. Lett.*, *16*, 609-612, 1989.

Loper, D.E., and T. Lay, The core-mantle boundary region, *J. Geophys. Res.*, *100*, 6397-6420, 1995.

Manga, M., Mixing of heterogeneities in the mantle - Effect of viscosity differences, *Geophys. Res. Lett.*, *23*, 403-406, 1996.

Masters, G., S. Johnson, G. Laske, and H. Bolton, A shear-velocity model of the mantle, *Phil. Trans. R. Soc. London A*, *354*, 1385-1410, 1996.

Monnereau, M., and M. Rabinowicz, Is the 670 km phase transition able to layer the Earth's convection in a mantle with depth-dependent viscosity?, *Geophys. Res. Lett.*, *23*, 1001-1004, 1996.

Nataf, H.C., and S. Houard, Seismic discontinuity at the top of D" - a worldwide feature?, *Geophys. Res. Lett.*, *20*, 2371-2374, 1993.

Olson, P., and C. Kincaid, Experiments on the interaction of thermal convection and compositional layering at the base of the mantle, *J. Geophys. Res.*, *96*, 4347-4354, 1991.

Osako, M., and E. Ito, Thermal diffusivity of $MgSiO_3$ perovskite, *Geophys. Res. Lett.*, *18*, 239-242, 1991.

Parmentier, E.M., C. Sotin, and B.J. Travis, Turbulent 3-D thermal convection in an infinite Prandtl number, volumetrically heated fluid - Implications for mantle dynamics, *Geophys. J. Int.*, *116*, 241-251, 1994.

Patankar, S.V., *Numerical Heat Transfer and Fluid Flow*, Hemisphere Publishing Corporation, New York, 1980.

Pollack, H.N., S.J. Hurter, and J.R. Johnson, Heat flow from the Earth's interior - Analysis of the global data set, *Rev. Geophys.*, *31*, 267-280, 1993.

Press, W.H., S.A. Teulolsky, W.T. Vetterling, and B.P. Flannery, *Numerical Recipes*, Cambridge University Press, Cambridge, UK, 1992.

Ratcliff, J.T., P.J. Tackley, G. Schubert, and A. Zebib, Transitions in thermal convection with strongly variable viscosity, *Phys. Earth Planet. Inter.*, *102*, 201-212, 1997.

Ricard, Y., M. Richards, C. Lithgow-Bertelloni, and Y. LeStunff, A geodynamic model of mantle density heterogeneity, *J. Geophys. Res.*, *98*, 21895-21909, 1993.

Robertson, G.S., and J.H. Woodhouse, dlnVs/dlnVp in the lower mantle and its mineral physics implications, *Eos Trans. AGU, Fall Meeting Suppl.*, *77*, 697, 1996.

Schubert, G., Numerical models of mantle convection, *Ann. Rev. Fluid Mech.*, *24*, 359-394, 1992.

Schubert, G., and P.J. Tackley, Mantle dynamics: The strong control of the spinel-perovskite transition at a depth of 660 km, *J. Geodynamics*, *20*, 417-428, 1995.

Sidorin, I., and M. Gurnis, Geodynamically consistent seismic velocity predictions at the base of the mantle, in *Observational and theoretical constraints on the core-mantle boundary region (this volume)*, edited by M. Gurnis, American Geophysical Union, 1998.

Sleep, N.H., Gradual entrainment of a chemical layer at the base of the mantle by overlying convection, *Geophys. J. Oxford*, *95*, 437-447, 1988.

Smolarkiewicz, P.K., A fully multidimensional positive definite advection transport algorithm with small implicit diffusion, *J. Comp. Phys.*, *54*, 325-362, 1984.

Solomatov, V.S., Scaling of temperature-dependent and stress-dependent viscosity convection, *Phys. Fluids*, *7*, 266-274, 1995.

Stacey, F.D., *Physics of the Earth*, Brookfield Press, Kenmore, Queensland, Australia, 1992.

Stevenson, D.J., Why D" is unlikely to be caused by core-mantle interactions (abstract), *Eos Trans. AGU, Fall Meeting Suppl.*, *74*, 51, 1993.

Stixrude, L., and M.S.T. Bukowinski, Fundamental thermodynamic relations and silicate melting with implications for the constitution of D'', *J. Geophys. Res.*, *95*, 19311-19325, 1990.

Su, W.J., R.L. Woodward, and A.M. Dziewonski, Degree-12 model of shear velocity heterogeneity in the mantle, *J. Geophys. Res.*, *99*, 6945-6980, 1994.

Tackley, P.J., Effects of strongly temperature-dependent viscosity on time-dependent, 3-dimensional models of mantle convection, *Geophys. Res. Lett.*, *20*, 2187-2190, 1993.

Tackley, P.J., Three-dimensional models of mantle convection: Influence of phase transitions and temperature-dependent viscosity, Ph.D. Thesis, California Institute of Technology, Pasadena, 1994.

Tackley, P.J., Effects of strongly variable viscosity on three-dimensional compressible convection in planetary mantles, *J. Geophys. Res.*, *101*, 3311-3332, 1996.

Tackley, P.J., D.J. Stevenson, G.A. Glatzmaier, and G. Schubert, Effects of an endothermic phase transition at 670 km depth in a spherical model of convection in the Earth's mantle, *Nature*, *361*, 699-704, 1993.

Tackley, P.J., D.J. Stevenson, G.A. Glatzmaier, and G. Schubert, Effects of multiple phase transitions in a 3-dimensional spherical model of convection in Earth's mantle, *J. Geophys. Res.*, *99*, 15877-15901, 1994.

van der Hilst, R.D., S. Widiyantoro, and E.R. Engdahl, Evidence for deep mantle circulation from global tomography, *Nature*, *386*, 578-584, 1997.

van Keken, P.E., S.D. King, H. Schmeling, U.R. Christensen, D. Neumeister, and M.-P. Doin, A comparison of methods for the modeling of thermochemical convection, *J. Geophys. Res.*, *102*, 22477-22496, 1997.

Vidale, J.E., and H.M. Benz, Seismological mapping of fine structure near the base of the Earth's mantle, *Nature*, *361*, 529-532, 1993.

Weinstein, S.A., and P. Olson, Planforms in thermal convection with internal heat sources at large Rayleigh and Prandtl numbers, *Geophys. Res. Lett.*, *17*, 239-242, 1990.

Wysession, M.E., Imaging cold rock at the base of the mantle: The sometimes fate of slabs?, *AGU Geophysical Monograph*, *96*, 369-384, 1996.

Yuen, D.A., O. Cadek, A. Chopelas, and C. Matyska, Geophysical inferences of thermal-chemical structures in the lower mantle, *Geophys. Res. Lett.*, *20*, 899-902, 1993.

Yuen, D.A., O. Cadek, P. van Keken, D.M. Reuteler, H. Kyvlova, and B.A. Schroeder, Combined results from mineral physics, tomography and mantle convection and their implications on global geodynamics, in *Seismic modeling of Earth structure*, edited by E. Boschi, G. Ekström, and A. Morelli, pp. 463-505, Instituto Nationale di Geofisica, Italy, 1996.

Zhang, S.X., and D.A. Yuen, The influences of lower mantle viscosity stratification on 3-D spherical-shell mantle convection, *Earth Planet. Sci. Lett.*, *132*, 157-166, 1995.

P.J. Tackley, Department of Earth and Space Sciences, University of California, Los Angeles, 405 Hilgard Avenue, Los Angeles, CA 90095-1567